Impact of urea-based deep eutectic solvents on Mg-MOF-74 morphology and sorption properties

Michaël Teixeira, Renata A. Maia, Sangaraju Shanmugam, Benoît Louis, Stéphane Baudron

Impact of urea-based deep eutectic solvents on Mg-MOF-74 morphology and sorption properties

Michaël Teixeira,[a] Renata A. Maia,[a] Sangaraju Shanmugam,[b] Benoît Louis[c,*] and Stéphane A. Baudron[a,*]

a. Université de Strasbourg, CNRS, CMC UMR 7140, 4 rue Blaise Pascal, F-67000 Strasbourg, France. E-mail : sbaudron@unistra.fr

b. Department of Energy Science and Engineering, Daegu Gyeongbuk Institute of Science & Technology (DGIST), 50-1, Sang-Ri, Hyeonpung-Myeon, Dalseong-Gun, Daegu 42988, The Republic of Korea

c. Université de Strasbourg, CNRS, ICPEES UMR 7515, 25 rue Becquerel, F-67087 Strasbourg, France. E-mail : blouis@unistra.fr

Abstract

Deep eutectic solvents (DES) based on different urea derivatives have been demonstrated to be efficient green alternatives for the ionothermal synthesis of the prototypical Mg-MOF-74 with a strong impact on the morphology and sorption properties of the material. While the synthesis of the material is rather straightforward in the reline (choline chloride:urea 1:2) DES, higher temperatures and longer reaction times are necessary in the e-urea (2-imidazolidinone, ethylene-urea) based analogous system. Interestingly, in the latter, a variety of intermediate crystalline phases could be observed and characterized by single-crystal X-ray diffraction. In these compounds, coordination of the DES components – the chloride anion and e-urea derivative – to the Mg(II) cation was found to compete with the carboxylate linker. It was rationalized that the difference in the synthesis conditions and in the isolation of intermediate systems originate from the varying decomposition kinetics of the DES and hence from the basicity of the solvent. Although the same material is obtained as ascertained by powder X-ray diffraction and elemental analysis, the final morphology characterized by SEM and TEM is dependent on the nature of the solvent. Whereas the classical rod-like shape is observed in reline, an unusual morphology showing slices perpendicular to the main growth axis is present in the e-urea based DES. For the

material featuring this unusual morphology, a higher specific surface area and CO_2 uptake were found, which were associated with a higher degree of microporosity.

Keywords

Deep eutectic solvents; Metal-organic frameworks; Ionothermal synthesis; CPO-27; MOF-74

Graphical abstract

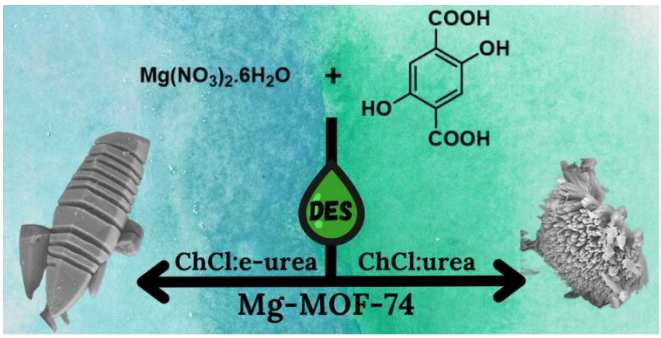

Highlights:

- The ionothermal synthesis of the Mg-MOF-74 has been performed in deep eutectic solvents.
- The nature of the urea derivative of the DES component is shown to impact the crystal morphology.
- The e-urea based DES leads to a material with an unusual morphology, higher specific surface area and CO_2 uptake capacity.

1. Introduction

Owing to their diverse and promising applications in gas storage and separation, heterogeneous catalysis or electronics among others,[1-3] Metal-Organic Frameworks (MOFs) have been the object of intense research over the past decades. The preparation of these crystalline porous materials is based on the assembly of organic ligands with metallic nodes, performed via mechanochemistry, ultrasounds, microwaves or solvothermal synthesis.[4-7] Not only the synthetic method employed can determine the nature and purity of the material obtained but also its crystallinity and properties. The most frequently applied approach remains solvothermal synthesis, consisting in heating, under autogenous pressure, the MOF precursors in a solvent or a mixture thereof. As it is often performed in solvents such as N,N'-dimethylformamide (DMF), N,N'-diethylformamide (DEF) or N,N-dimethylacetamide (DMA) that are toxic and flammable, others have been sought, as illustrated by the emergence of the use of green systems[8-11] and of the ionothermal strategy.[12-16] In this context, ionic liquids and their cousins, deep eutectic solvents (DESs), have been explored. DESs are the combination of two or more solids, often hydrogen bond donor/acceptor, affording a system with a melting point below the one of each of their components.[17-24] DESs feature a wide liquid range, non-flammability, low vapor pressure and the ability to dissolve polar species, making them an appealing synthetic media. The 1:2 combinations of choline chloride (ChCl, Scheme 1) with urea derivatives[25,26] have been particularly investigated for the preparation of MOFs and have been shown to play a diversity of roles.[16,27] For example, one of the components of the solvent that can be neutral (urea derivative), anionic (chloride) or cationic (cholinium) may be coordinated to the metal centers or present within the pores of the MOFs.[27] Furthermore, we have recently reported that the ChCl:urea (1:2) DES, known as reline,[25] can induce the conversion of HKUST-1 into another structure and that it can impact its crystal morphology and textural properties.[28] Hence, a rose-like morphology was obtained, contrasting with the expected octahedral shape for this Cu-based material.[29] In light of this result, it appeared of interest to investigate the impact of these synthetic conditions on other prototypical MOFs like the M_2(dobdc) series (dobdcH_4 = 2,5-dihydroxyterephthalic acid, Scheme 1).[30-35] Known as MOF-74[30] or CPO-27[31], this class of materials exhibits fascinating characteristics as highlighted by the high porosity and surface area and sorption properties towards CO_2 and CH_4 of Mg-MOF-74.[32-35] While the preparation of this MOF has been described in different systems,[35-36] the use of DES has not been reported.

As a matter of fact, the ionothermal approach remains more generally underexplored for Mg based MOFs with, to the best of our knowledge, only few reports focussing on ionic liquids.[37,38] We therefore report herein on the unprecedented use of the ChCl:urea and ChCl:e-urea (1:2) DESs (e-urea = 2-imidazolidinone, ethylene urea, Scheme 1) as viable solvents for the preparation of Mg-MOF-74, and on the influence of the nature of the urea derivatives on the crystal morphology and size, textural and sorption properties of the material.

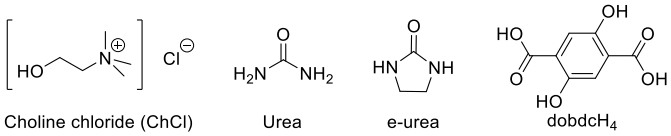

Choline chloride (ChCl) Urea e-urea $dobdcH_4$

Scheme 1. Representations of DES components and of the $dobdcH_4$ ligand.

2. Experimental section

2.1. Materials

All chemicals were obtained from commercial sources and were used as received. The DES components where individually weighted and placed in a round bottom flask equipped with a magnetic bar. For both DES, ChCl:urea and ChCl:e-urea, a 1:2 molar ratio was used. The mixture was then stirred and heated at 100 °C under ambient atmosphere until a homogeneous and clear liquid phase was obtained, which typically takes up to 30 minutes or less. The solvent was freshly prepared before each reaction.

2.2. Synthesis

Synthesis of Mg-MOF-74 in choline chloride:urea (1:2):

0.396 g (2 mmol) of 2,5-dihydroxyterephthalic acid and 1.026 g (4 mmol, 2 equiv.) of $Mg(NO_3)_2 \cdot 6H_2O$ were added to a 48 mL Chemglass® high-pressure vessel. Then, 25 mL of freshly prepared choline chloride:urea 1:2 DES was added with the aid of a syringe, and the vessel was closed with its Teflon cork. The vial was heated for 2 days at 120 °C. After completion of the reaction, the content of the vessel was mixed with water (20 mL) and centrifuged. The recovered solid was washed 2 more times with water (2x20 mL) and 3 times with ethanol (3x20 mL). The solid was air-dried overnight and 0.428 g were obtained (51.7% relative to the $Mg_2(dhtp)(H_2O)_{9.5}$ formula). Elemental analysis (CHN) for $C_8H_{21}Mg_2O_{15.5}$ ($[Mg_2(dobdc)(H_2O)_{9.5}]$), calculated: C, 23.22%; H, 5.11%; N, 0%; found: C, 23.29%; H, 4.99%; N, 0%.

Synthesis of Mg-MOF-74 in choline chloride:e-urea (1:2):

0.396 g (2 mmol) of 2,5-dihydroxyterephthalic acid and 1.026 g (4 mmol, 2 equiv.) of $Mg(NO_3)_2 \cdot 6H_2O$ were added to a 48 mL Chemglass® high-pressure vessel. Then, 25 mL of freshly prepared choline chloride:e-urea 1:2 DES was added with the aid of a syringe, and the vessel was closed with its Teflon cork. The vial was then heated for 3 days at 140 °C. After completion of the reaction, the content of the vessel was mixed with water (20 mL) and centrifuged. The recovered solid was washed 2 more times with water (2x20 mL) and 3 times with ethanol (3x20 mL). The solid was air-dried overnight and 0.244 g were obtained (29.8% relative to the $Mg_2(dobdc)(H_2O)_9(e\text{-}urea)_{0.05}$ formula). Elemental analysis (CHN) for $C_{8.15}H_{20.3}Mg_2N_{0.1}O_{15.05}$ ($[Mg_2(dobdc)(H_2O)_9(e\text{-}urea)_{0.05}]$), calculated: C, 23.93%; H, 5.00%; N, 0.34%; found: C, 23.77%; H, 4.95%; N, 0.42%.

Compounds **1**-**4** were isolated from batches obtained when performing the reaction at 80 °C, 100 °C or 120 °C. Owing to the sensitivity to water, the compounds were solely washed with EtOH and crystals were picked from the mixtures for structure determination by X-ray diffraction. As the compounds were obtained in mixtures with other unidentified species, further characterization beyond their crystal structure determination could unfortunately not be performed.

Synthesis of Mg-MOF-74 in choline chloride:e-urea 1:2 with addition of ethylenediamine:

2,5-dihydroxyterephthalic acid and $Mg(NO_3)_2 \cdot 6H_2O$ were added to a vial. Then, ethylenediamine and the freshly prepared choline chloride:e-urea 1:2 DES was added with the aid of a syringe, and the vessel was closed with its Teflon cork and then heated for 2 days (see experimental details in Table 1). After completion of the reaction, the content of the vessel was mixed with water (4 mL) and centrifuged. The recovered solid was washed 2 more times with water (2x20 mL) and 3 times with ethanol (3x20 mL). The solid was air-dried overnight.

Table 1. Experimental conditions for the Mg-MOF-74 synthesis in the choline chloride:e-urea 1:2 DES with addition of ethylenediamine.

Entry	$Mg(NO_3)_2 \cdot 6H_2O$ (mmol)	dobdc (mmol)	Ethylenediamine (mmol)	DES (mL)	T (°C)
1	0.4	0.2	0.02 (0.1 equiv.)	2.5	120
2	0.4	0.2	0.2 (1 equiv.)	2.5	120
3	0.2	0.1	0.01 (0.1 equiv.)	1.25	140
4	0.2	0.1	0.1 (1 equiv.)	1.25	140
5[a]	-	-	0.05 (1 equiv.)	1.25	140

[a] Instead of adding 2,5-dihydroxyterephtalic acid and $Mg(NO_3)_2 \cdot 6H_2O$, it was added 0.02 g of Mg-MOF-74 (0.05 mmol, assuming the molecular weight of 409.15 g/mol for the formula $[Mg_2(dobdc)(H_2O)_9(\text{e-urea})_{0.05}]$) previously made in ChCl/e-urea.

2.3. Elemental analysis

Elemental analyses (CHN) were performed at the *Service Commun d'Analyses* of the University of Strasbourg, in duplicate, employing a ThermoFischer Flash 2000 equipment. The reported values for the CHN were taken as the average of two measurements.

2.4. Thermogravimetric analysis and differential scanning calorimetry

The thermal stability of the samples was accessed in a PerkinElmer Thermogravimetric Analyzer TGA 4000 under N_2 flow of 20 mL/min, and a heating rate of 5°C/min up to 800°C. The differential scanning calorimetry study was performed on a PerkinElmer Jade DSC under N_2 flow of 20 mL/min and a heating rate of 5°C/min up to 450°C.

2.5. Scanning electron microscopy

SEM images were obtained with a Zeiss GeminiSEM 500 microscope with a FEG Schottky source and an Everhart–Thornley detector.

2.6. High-resolution transmission electron microscopy

HRTEM images were acquired after the dispersion of the samples in ethanol, sonication for a few seconds, and drop-deposition on a copper grid with a holey carbon film over a Hitachi HF-3300kV instrument.

2.7. X-ray diffraction

Table 2. Crystallographic data for **1**-**4**.

	1	**2**	**3**	**4**
Formula	$C_{18}H_{36}Cl_2MgN_{12}O_6$	$C_{24}H_{48}Cl_2MgN_{16}O_8$	$C_{26}H_{40}MgN_{12}O_{12}$	$C_{20}H_{28}MgN_8O_{10}$
FW	611.80	783.99	822.85	564.81
Crystal system	monoclinic	monoclinic	triclinic	triclinic
Space group	*I*2/*a*	$P2_1/c$	*P*-1	*P*-1
a, Å	18.3027(8)	9.6056(3)	9.0116(5)	7.2644(3)
b, Å	10.6875(4)	8.8329(4)	9.1303(4)	9.0338(3)
c, Å	29.9973(15)	21.4198(8)	10.1604(6)	10.4608(4)
α, °			86.650(2)	70.3280(10)
β, °	107.198(3)	98.768(2)	82.468(3)	78.291(2)
γ, °			89.652(3)	67.7950(10)
V, Å^3	5522.7(4)	1796.13(12)	827.35(8)	596.22(4)
Z	8	2	1	1
T, K	173(2)	173(2)	173(2)	173(2)
μ, mm^{-1}	0.316	0.267	0.135	0.150
Refls. coll.	57276	20541	17812	23564
Ind. refls. (R_{int})	8080 (0.1873)	5140 (0.0597)	4547 (0.0580)	3236 (0.0500)
R_1 (I>2σ(I))[a]	0.1228	0.0471	0.0481	0.0383
wR_2 (I>2σ(I))[a]	0.2453	0.1253	0.1253	0.1027
R_1 (all data)[a]	0.1613	0.0607	0.0595	0.0411
wR_2 (all data)[a]	0.2618	0.1360	0.1352	0.1051
GOF	1.162	1.027	1.031	1.066

[a] $R_1 = \sum||F_o| - |F_c||/\sum|F_o|$; $wR_2 = [\sum w(F_o^2-F_c^2)^2/\sum wF_o^4]^{1/2}$

Data (Table 2) were collected at 173 K on a Bruker SMART CCD diffractometer with Mo-Kα radiation. Both structures were solved using SHELXS-97 and refined by full matrix least-squares on F^2 using SHELXL-2016 with anisotropic thermal parameters for all non-hydrogen atoms.[39] The hydrogen atoms were introduced at calculated positions and not refined (riding model). CCDC 2164716-2164719.

X-ray diffraction powder patterns were recorded at 293 K on a Bruker D8 diffractometer using monochromatic Cu-Kα radiation with a scanning range between 4 and 40° using a scan step of 1.2°/min. The simulated diagrams were generated with the Mercury® software based on the single-crystal data collected at 173 K.

2.8. Gas sorption

The textural properties and CO_2 uptakes of the samples were obtained by adsorption-desorption isotherms with N_2 at 77 K and CO_2 at 273 K, respectively, in a Micromeritics ASAP 2020 Surface Area and Porosity Analyzer. The Brunauer-Emmett-Teller (BET) method was used for obtaining the specific surface area, and the total pore volume (V_{Total}) was obtained by single point adsorption at $p/p_0 \approx 0.97$. The t-plot method was employed for obtaining the micropore volume (V_{Micro}) and the specific surface area related to the micropores ($S_{BET,Micro}$). The samples were outgassed, prior to the N_2 and CO_2 adsorption-desorption analysis, by heating the sample under vacuum at 250°C for 12 h, and the MicroActive Software version 4.00 was used to analyze the data.

3. Results and discussion

3.1. Synthesis of Mg-MOF-74 in reline

The preparation of Mg-MOF-74 has been initially studied in ChCl:urea (1:2) (reline), and then extended to the e-urea-based solvent. The synthetic conditions explored consisted in heating a 2 to 1 molar mixture of the $Mg(NO_3)_2.6(H_2O)$ salt and the $dobdcH_4$ ligand (Scheme 1) in the DES at temperatures ranging from 80 °C to 140 °C, over 1 to 10 days, followed by washing with water and ethanol. In reline, Mg-MOF-74 formed even at 80 °C and after one day albeit with low yields. Both the yield and crystallinity, assessed by X-ray diffraction, were improved upon performing the reaction at 120 °C over two days. As presented in Fig. 1, X-ray powder diffraction confirms the successful preparation of the desired material. Furthermore, elemental analysis gave the

formulation $Mg_2(dobdc).(H_2O)_{9.5}$ as expected for Mg-MOF-74. The absence of nitrogen is worth emphasizing, thereby demonstrating the efficiency of the work-up method for removal of urea and of the cholinium cation. Thermogravimetric analysis (Fig. 2) showed a first weight loss around 80 to 100 °C corresponding to the water molecules present in the pores followed by a plateau up to 400°C. This is consistent with what has been reported for Mg-MOF-74 in the literature.[32] Both materials showed similar behaviour by differential scanning calorimetry (Fig. SM3).

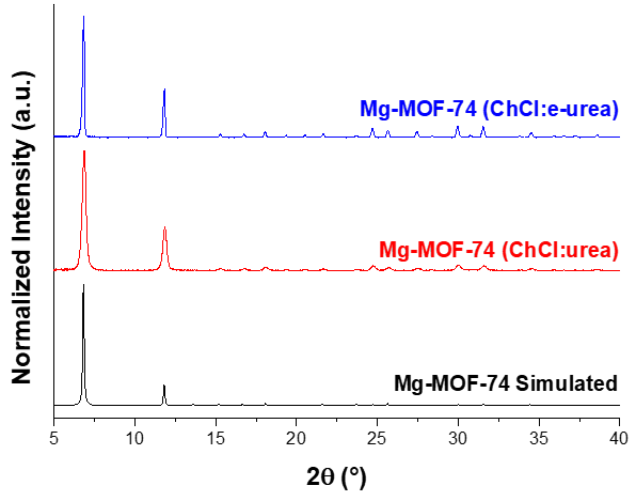

Fig. 1. X-ray powder pattern of Mg-MOF-74 prepared from reline or ChCl:e-urea (1:2) and comparison with the simulated powder pattern for this material.

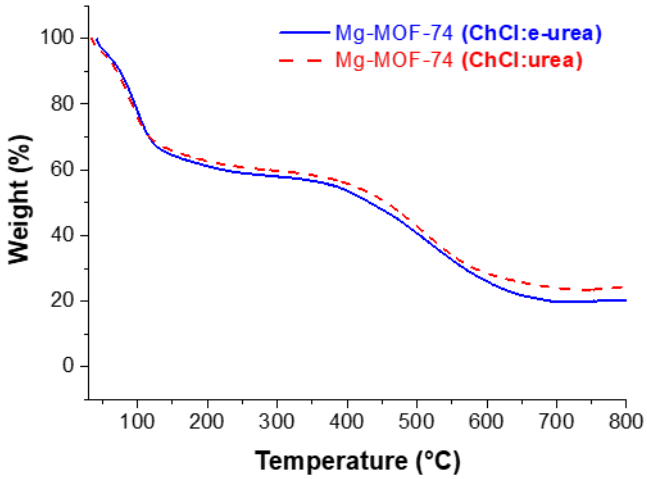

Fig. 2. Thermogravimetric analysis of Mg-MOF-74 prepared from reline or ChCl:e-urea (1:2).

3.2. Synthesis of Mg-MOF-74 in ChCl:e-urea

When performing the synthesis of the MOF in the ChCl:e-urea (1:2) DES by heating at 80 °C, 100 °C or 120 °C and for up to 10 days, a mixture of varying crystalline compounds, including Mg-MOF-74, formed. Since the crystalline materials other than the desired MOF were found to be unstable upon washing with water, only ethanol was employed to recover them before their characterization by powder X-ray diffraction, revealing complex diffractograms. Interestingly, some of those compounds were isolated as large single crystals allowing their structure determination.

3.2.1. Intermediate phases

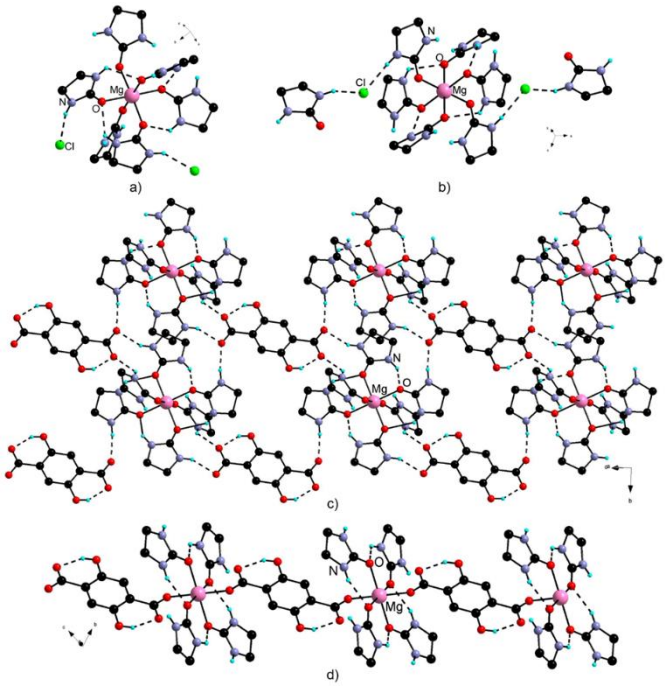

Fig. 3. Crystal structure of complexes **1** (a), **2** (b), **3** (c) and 1D coordination polymer **4** (d). CH hydrogen atoms have been omitted for clarity.

One of the major products recurrently isolated is $[Mg(e\text{-urea})_6]Cl_2$, **1**, crystallizing in the monoclinic *I*2/*a* space group (see Table 2). In this mononuclear complex, the Mg(II) cation adopts an octahedral environment by coordination to six e-urea molecules with Mg-O distances ranging from 2.057(4) to 2.074(4) Å (Fig. 3a). Charge compensating chloride anions are hydrogen bonded to the N-H moieties leading to a 3-dimensional arrangement. An e-urea solvate of this complex, formulated $[Mg(e\text{-urea})_6]Cl_2(e\text{-urea})_2$, **2**, crystallizing in the monoclinic $P2_1/c$ space group (see

Table 2) could also be characterized. A similar coordination sphere of the Mg(II) cation is observed for **2** (d_{Mg-O} = 2.0366(11) to 2.0894(11) Å) (Fig. 3b). However, the presence of these two compounds does not account for all the peaks observed in the X-ray powder pattern collected on the reaction batches (as illustrated for reactions at 120 °C in Fig. SM1) suggesting that other phases are also formed either with components of the solvent or with the dobdcH_4 ligand. The preferred interaction of the DES with the alkaline earth metal cation was confirmed by running reactions in the absence of the dobdcH_4 ligand. Upon heating the $Mg(NO_3)_2.6(H_2O)$ salt in the e-urea based solvent at 120 °C for 10 days, crystalline material could indeed be harvested exhibiting a diffractogram analogous to the ones obtained when performing the reaction in the presence of dobdcH_4 below 140 °C (see Fig. SM1).

While the [Mg(e-urea)$_6$]Cl_2 salts and solvent based materials described above are predominant for reactions at 80 °C, two other crystalline species could be isolated and characterized by single-crystal X-ray diffraction upon increasing the temperature and lengthening the reaction time. First, mononuclear complex [Mg(e-urea)$_6$](dobdcH_2), **3**, crystallizing in the triclinic space group *P*-1 (Table 2), was obtained at 100 °C, and in increasing amount as reaction time lengthened. It comprises the same octahedral $[Mg(e\text{-urea})_6]^{2+}$ species (d_{Mg-O} = 2.0497(11) to 2.0859(10) Å) but with $(dobdcH_2)^{2-}$ as charge-compensating anion (Fig. 3c). The two carboxylate units are hydrogen bonded intramolecularly to the two hydroxyl groups and intermolecularly to e-urea N-Hs.

Interestingly, for longer reaction durations at 100 °C, a one-dimensional coordination polymer [Mg(dobdcH_2)(e-urea)$_4$], **4** (Triclinic, *P*-1, Table 2) also formed. In this compound, four e-urea molecules occupy the square base of the octahedral coordination sphere of the alkaline earth cation (d_{Mg-O} = 2.0845(8) to 2.1136(8) Å) while the two remaining axial positions are occupied by bridging $(dobdcH_2)^{2-}$ anions (d_{Mg-O} = 2.0409(9) Å) (Fig. 3d). This one-dimensional network was also found upon performing the reaction at 120 °C for few days, whereas Mg-MOF-74 remains the major product for longer reaction duration at this temperature. While **4** is structurally reminiscent of the reported [M(dobdcH_2)(H_2O)$_4$] (M = Ni, Co) chains,[40] it is worth noting that intermediate phases on the way to Mg-MOF-74 have been recently described showing also deprotonation solely at the carboxylate units.[41] Partial deprotonation to the dobdcH_2 ligand has also been observed for Ca-MOFs prepared in the ChCl:e-urea (1:2) DES.[42]

3.3.2. Mg-MOF-74 phase

When the synthesis is performed at 140 °C, Mg-MOF-74 is almost exclusively obtained with minor amounts of the chloride-based phases that can be easily removed by washing with water. Therefore, the conditions employed to obtain the desired material in pure form consisted in heating at 140 °C for 3 days followed by water and EtOH washing. X-ray powder diffraction (Fig. 1) and elemental analysis, indicating the formula $Mg_2(dobdc)(H_2O)_9(e\text{-}urea)_{0.05}$, confirmed the preparation of the Mg-MOF-74. It can be noted here that, in this solvent, a small percentage of nitrogen is found in the analysis suggesting the presence of e-urea within the material. Thermogravimetric analysis for this material shows a behaviour analogous to what has been observed for the compound prepared from reline (Fig. 2).

3.3. Crystal morphology

The SEM micrographs of the two materials reveal striking different morphologies. For Mg-MOF-74 prepared in reline, aggregates of hexagonal rods are observed (Figs. 4a and b), as reported in the literature for common synthetic methods.[36,43] The material prepared in the ChCl:e-urea DES presents a strikingly different morphology, as it forms 1 to 20 µm long crystals with a hexagonal shape but featuring slicing (Figs. 4c,d). Such morphology showing slices perpendicular to the main growth axis will be hereafter coined shish-kebab like. Shish-kebab organization is sometimes observed in the crystallization of polymers with transverse lamellae growing from a central thread.[44] These slices are here randomly distributed across the crystal length, as some crystals exhibit up to several dozens of them. It is rationalized that these motifs significantly increase the exposed surface of the crystals thus leading to more exposed micropores, in line with the gas sorption measurements (*vide infra*).

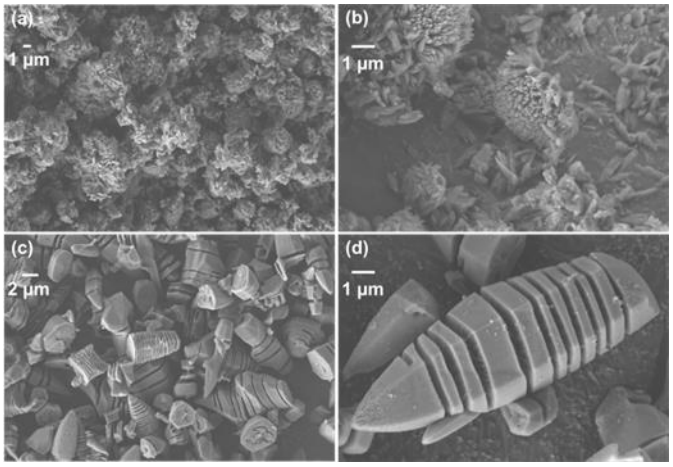

Fig. 4. SEM micrographs of Mg-MOF-74 prepared in reline (a, b) or ChCl:e-urea (1:2) (c, d).

The unusual morphology of the Mg-MOF-74 prepared in the ChCl:e-urea DES was further investigated by high-resolution TEM. According to Fig. 5, it is possible to visualize that this unusual porous morphology seems to be originating from a twisted arrangement of this crystal. Furthermore, the HRTEM coupled with energy-dispersive X-ray spectroscopy (EDX) confirmed that such morphology is indeed attributed to the Mg-MOF-74 material, given the homogeneous presence of the elements Mg, C, and O throughout the sample (Fig. 6).

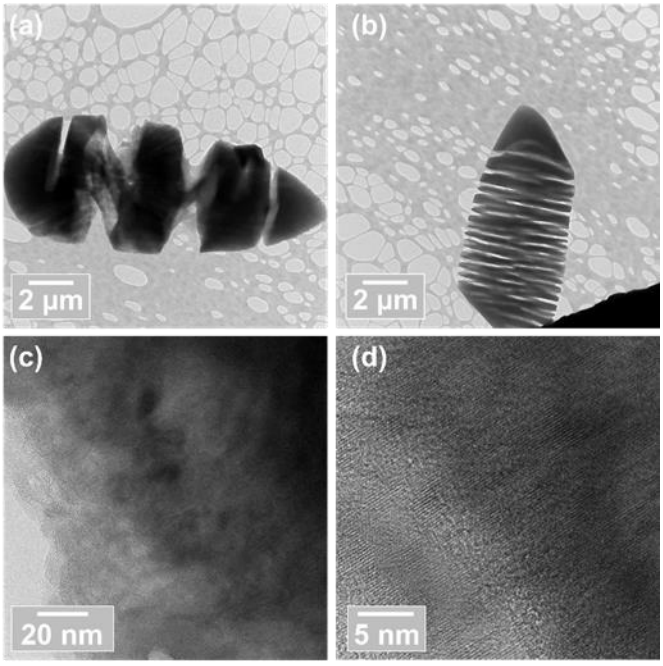

Fig. 5. HRTEM micrographs of Mg-MOF-74 prepared in ChCl:e-urea (1:2) (a-d).

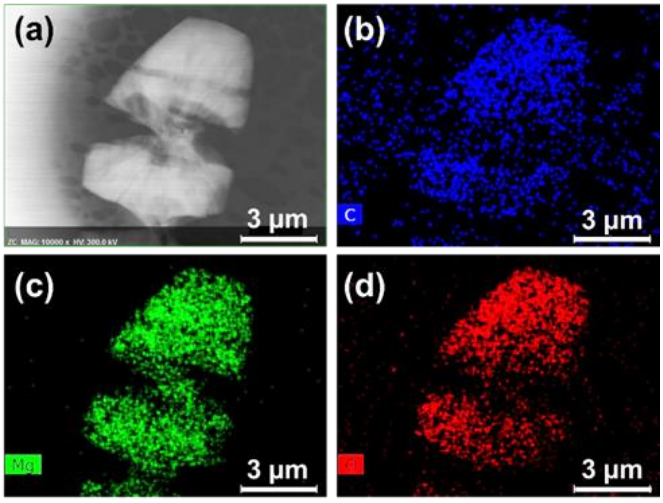

Fig. 6. HRTEM-EDX micrographs of Mg-MOF-74 prepared in ChCl:e-urea (1:2) for the elements C (b), Mg (c), and O (d).

3.4. DES role regarding the Mg-MOF-74 formation

These observations in the crystal morphologies suggest that the nature of the solvents is responsible for such differences. Such a phenomenon is difficult to precisely rationalize but may be related to the varying intrinsic physical and chemical properties of these two solvents. Indeed, whereas reline has a melting point at 12 °C, the one of the ChCl:e-urea (1:2) DES is substantially above room temperature, 70 °C,[26] which is in agreement with the visual observation that the latter solvent is much more viscous than the former at the same working temperatures. Furthermore, reline is known to exhibit decomposition upon heating, with urea converting into ammonia (Scheme 2a).[45] For example, it has been found that 0.1% of ammonia formed upon heating reline for 7 hours at 80 °C. The decomposition process is further promoted by the presence of alcohols, temperature and time. For the ChCl:e-urea (1:2) DES, such decomposition yielding ethylenediamine[26] is expected to be substantially slower (Scheme 2b, for a proposed potential decomposition pathway), according to the known slower thermal decomposition of the similar DES ChCl:m-urea (N,N'-dimethylurea) into methylamine.[45] Hence, these two DESs also vary in their basicity over time due to their varying nature and the particular kinetics of their thermal decomposition.

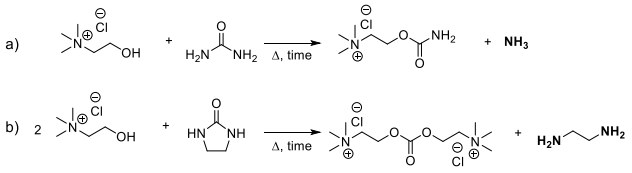

Scheme 2. Thermal decomposition over time of reline [45] (a) and a proposed thermal decomposition pathway for ChCl:e-urea (b).

A parallel can be drawn with the use of DMF and DEF for the MOF solvothermal synthesis, where the solvent decomposition releases basic amines favouring deprotonation of the bridging ligand and subsequently MOF formation. In reline, decomposition of the solvent combined with its lower viscosity may lead to faster MOF synthesis than in the e-urea based medium. Upon initial dissolution of the Mg(II) salt in this DES, formation of e-urea coordinated complexes is immediate, thus leading to the formation of compounds incorporating components of the DES such as $[Mg(e\text{-}urea)_6]Cl_2$ **1** and $[Mg(e\text{-}urea)_6]Cl_2(e\text{-}urea)_2$ **2**. As temperature increases and the reaction duration lengthens, the $dobdcH_4$ ligand is deprotonated (at the carboxylic acid function) thus competing

with the e-urea for the coordination sphere of the alkaline earth metal cation to afford complex **3** $[Mg(e\text{-}urea)_6](dobdcH_2)$, coordination polymer $[Mg(dobdcH_2)(e\text{-}urea)_4]$ **4** and eventually Mg-MOF-74. These various isolated phases and their sequence of formation are consistent with the proposed analysis, although the whole mechanism may be more complex and needs to be further elucidated. This rationale is nonetheless in line with the recently reported stepwise deprotonation of the ligand upon performing the synthesis of Mg-MOF-74 in DMF/ethanol/water with high concentration of the reagents leading to the isolation of previously unobserved carboxylate-only coordination polymers.[41]

From a morphological point of view, this modular growth of Mg-MOF-74 in ChCl:e-urea is also aligned with the findings of the Zhou group for the MOF-74-II material.[46] The reported MOF-74-II was prepared in DEF by the reaction between zinc nitrate and linker II (3,3'-dihydroxy-[1,1'-biphenyl]-4,4'-dicarboxylic acid), an elongated version of the $dobdcH_4$ ligand. Triggered by the unusual hollow nanotube morphology observed for this MOF, the authors reverse-engineered its assembly by a series of systematic studies and demonstrated that the slow release of diethylamine, generated by the thermal decomposition of DEF, was responsible for the selective deprotonation of the ligand linker II. First, the deprotonation of the carboxylic acid moieties led to the formation of a labile phase called PCN-74 (dense nanotube), where the free carboxylate group coordinates with the Zn^{2+} ion without the participation of the phenolic groups. As greater quantities of diethylamine are released in the reaction system, the less acidic protons (phenolic) are deprotonated, which enables these phenolate moieties to participate in the coordination sphere of zinc and to further form the MOF-74-II material. This growth was rationalized as occurring on the surface of the dense nanotube originated from the labile phase of PCN-74. Gradually, this metastable PCN-74 phase dissolves to afford the MOF-74-II material as a hollow nanotube morphology. Furthermore, this labile phase-assisted growth of MOF-74-II was elegantly demonstrated by artificially adding varying amounts of diethylamine into the reaction system (0.16 – 1.6 equiv.), in which small amounts of it generated firstly the PCN-74 phase, while greater amounts led directly to the MOF-74-II formation.

Likewise, in order to verify whether this selective deprotonation was taking place in our reaction and impacting the final morphology for the ChCl:e-urea system, we purposely added 0.1 – 1.0 equiv. of ethylenediamine in the reaction system at 140 °C (Table 1, Entries 3 and 4). As can be seen in Fig. 7, when 0.1 equiv. of ethylenediamine is added, both morphologies, the sliced one and

the traditional hexagonal rods, are present. On the other hand, when 1.0 equiv. of ethylenediamine is added (Fig. 8), there is – almost predominantly – the sole presence of the traditional hexagonal rod morphology. Interestingly, there is some reminiscent long crystals with just a few slicing (Fig. 8d), as if the evolution of the shish-kebab morphology was stopped midway its formation. When trying to perform the same experiment at 120 °C (Table 1, Entries 1 and 2), no product could be recovered when 0.1 equiv. of ethylenediamine was added, whereas the typical morphology of hexagonal rods was observed for the addition of 1.0 equiv. of the base.

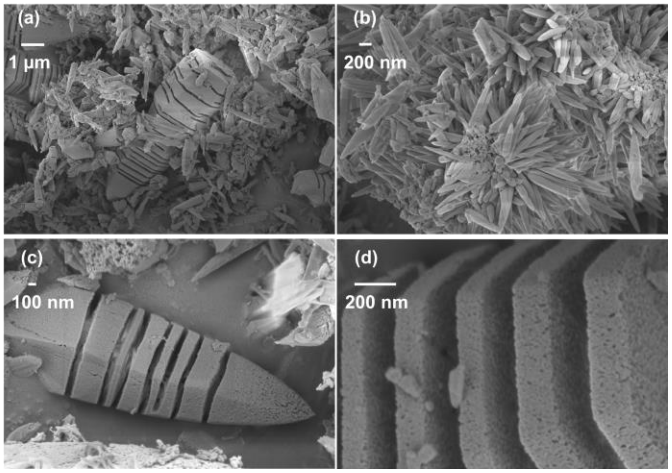

Fig. 7. SEM micrographs of Mg-MOF-74 prepared in ChCl:e-urea (1:2) with addition of 0.1 equiv. of ethylenediamine.

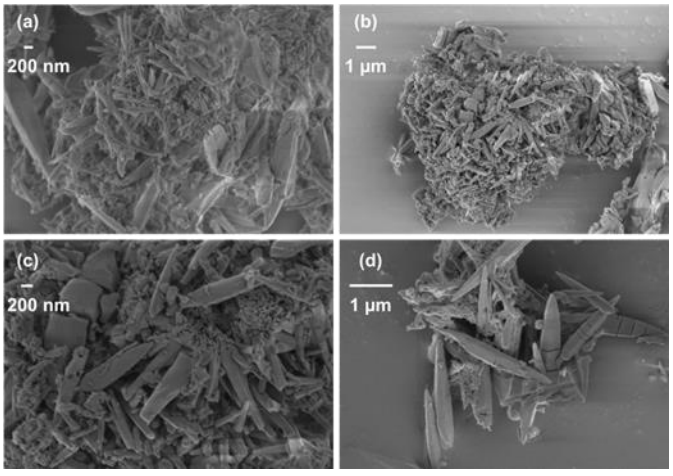

Fig. 8. SEM micrographs of Mg-MOF-74 prepared in ChCl:e-urea (1:2) with addition of 1.0 equiv. of ethylenediamine.

Finally, we tried to immerse the already-prepared Mg-MOF-74 with the unique sliced morphology in the ChCl:e-urea solvent with addition of 1.0 equiv. of ethylenediamine (Table 1, Entry 5). The surface of the material appeared to have suffered erosion, but the overall morphology aspect remained the same (Fig. 9).

All in all, the results of these experiments indicate that the kinetics of the base release from the DES (by thermal decomposition) has a significant impact on both MOF formation and morphology. Such features may also be impacted by (i) the viscosity of DESs, which has a potential impact on the diffusion of the reactants during the reaction time; and (ii) the DES stabilization of water-sensitive materials, which allows the formation of MOFs that are usually prone to hydrolysis.[28,42,47] Thus, we hypothesize that a labile phase may be produced in the initial stages of MOF formation, this phase may assist the assembly of the sliced morphology for Mg-MOF-74, in a similar way as the PCN-74 assisted the formation of Mg-MOF-74-II. This hypothesis is also in accordance with the above-mentioned recent report of intermediate phases towards Mg-MOF-74 incorporating the ligand exclusively deprotonated at the carboxylic acid moieties when using a higher concentration of the reagents in DMF/ethanol/water.[41] However, further studies need to be done to fully elucidate the proposed morphology formation mechanism in the ChCl:e-urea DES.

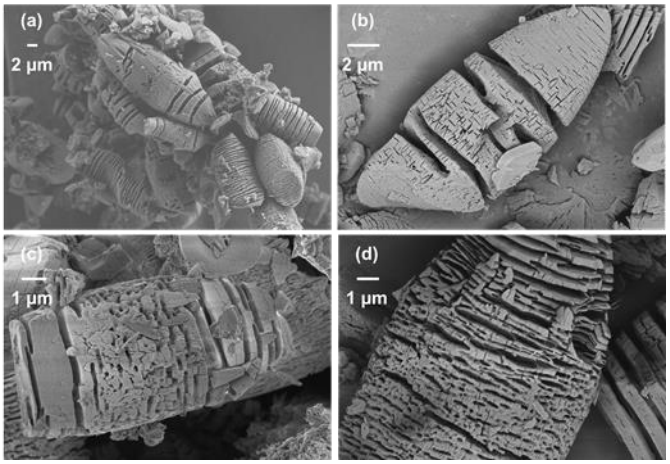

Fig. 9. SEM micrographs of the already-prepared shish-kebab Mg-MOF-74 immersed in ChCl:e-urea (1:2) with addition of 1.0 equiv. of ethylenediamine.

3.5. Textural properties and CO_2 uptake

While the Mg-MOF-74 prepared from the urea and e-urea based solvents exhibit analogous X-ray diffraction patterns (Fig. 1), we sought to investigate the impact of the crystal morphology on the sorption properties. Hence, they were analysed by N_2 adsorption-desorption isotherms at 77 K (Fig. 10). The specific surface area was calculated by the Brunauer–Emmett–Teller (BET) method (S_{BET}), and the total pore volume (V_{Total}) was obtained by single point adsorption ($p/p_0 \approx 0.97$) (Table SM1). The t-plot method was used to determine the micropore volume (V_{Micro}) and the specific surface area related to the micropores ($S_{BET,Micro}$). Prior to the gas sorption measurements, the materials were outgassed by heating them at 250 °C for 12 hours. Powder X-ray diffraction and TGA confirmed that the MOFs were unaltered by the outgassing process and the analysis. Interestingly, the two MOFs show different textural properties, as the material prepared form the e-urea based DES shows a much higher surface area compared with the analogue prepared from reline (1669 vs 996 $m^2.g^{-1}$) (Fig. 10). The S_{BET} of 1669 $m^2.g^{-1}$ is in the higher-end of what has been reported for this material.[32-36] It should be noted that analysis of different batches prepared in either the urea or e-urea based-DESs consistently afforded substantially larger surface areas for the MOFs prepared in the latter solvent.

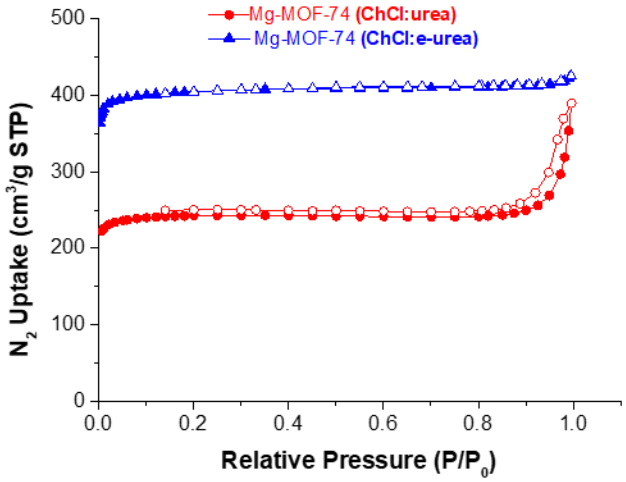

Fig. 10. N_2 adsorption-desorption isotherms at 77 K for Mg-MOF-74 prepared from reline (red circles) and from the ChCl:e-urea (1:2) DES (blue triangles). Closed symbols stand for adsorption and open ones stand for desorption.

The contribution of the microporosity to the specific surface area ($S_{BET,Micro}$) was found to be 1557 $m^2.g^{-1}$ and 940 $m^2.g^{-1}$, for the ChCl:e-urea- and reline-based materials, respectively. Mg-

MOF-74 prepared in ChCl:e-urea showed a classic type I isotherm, typical of a microporous material. For the MOF prepared in reline, a type I isotherm is also present, but with a mesoporous contribution indicated by a narrow hysteresis loop at the desorption branch between p/p_0 0.8-1.0. The V_{Micro} also evidences this feature, while the micropore volume contribution to the total pore volume of the reline-based MOF is 76% (V_{Micro} = 0.351 cm^3/g and V_{Total} = 0.460 cm^3/g), the same contribution related to the ChCl:e-urea DES-based MOF is 90% (V_{Micro} = 0.583 cm^3/g and V_{Total} = 0.645 cm^3/g). The high-contribution of the microporosity for the ChCl:e-urea-based system seems to be in agreement with our observations: whereas Mg-MOF-74 forms straightforwardly in reline, the formation of this material in ChCl:e-urea seems to go through a longer path and through several intermediates until MOF-74 formation, which would allow a slow maturation of the crystalline structure.

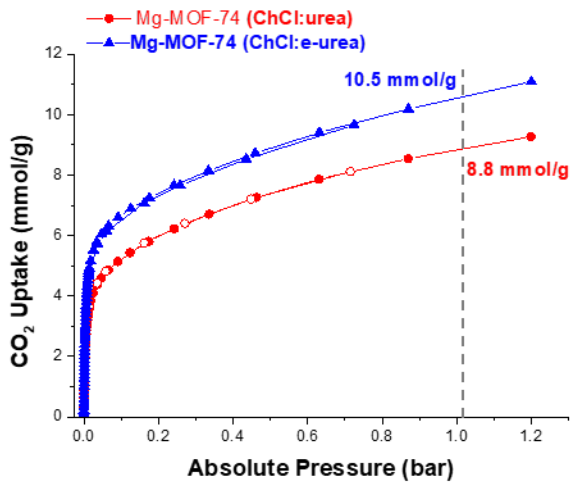

Fig. 11. CO_2 adsorption-desorption isotherms at 273 K for Mg-MOF-74 prepared from reline (red circles) and from the ChCl:e-urea (1:2) DES (blue triangles). Closed symbols stand for adsorption and open ones stand for desorption.

The Mg-MOF-74 is one of the most studied MOFs regarding CO_2 adsorption due to its open metal sites (OMS).[48,49] Consequently, the sorption properties for the MOF materials prepared with reline and ChCl:e-urea DESs were investigated by performing adsorption-desorption isotherms at 273 K in the 0-1.2 bar pressure range (Fig. 11). Their CO_2 uptake capacities at 1 bar were estimated as 8.8 mmol/g and 10.5 mmol/g, for the reline and the ChCl:e-urea-based DESs, respectively. The CO_2 uptake of the ChCl-e-urea-based Mg-MOF-74 was in the same range of the

highest reported values for such MOF at 273 K and 1 bar (9.4 mmol.g^{-1} and 10.2 mmol.g^{-1}).[50,51] Additionally, the steep slope at the low-pressure region of the isotherms represents a strong adsorption of the CO_2 molecule on the OMSs,[51,52] and the reversibility of the isotherms is granted by the overlap of the adsorption and desorption branches, which indicates the complete regeneration of the sorbent after the desorption process. The values found for the CO_2 uptake for these MOFs are in agreement with its N_2 sorption data, where a higher contribution of the microporosity for the ChCl:e-urea-based MOF provided a higher specific surface area and, consequently, a higher CO_2 uptake of roughly 20%.

Given the unusual sliced morphology of this MOF and considering that the diffusion length for a Ni-MOF-74[53] was shown to be morphology-dependent – hollow Ni-MOF-74 were shown to exhibit a 54% faster diffusion rate compared to fully solid ones – we believe that the CO_2 diffusion properties of this shish-kebab-like Mg-MOF-74 are a domain worth further investigating. Indeed, Gao *et al*. overviewed that the CO_2 capture capacity in a given MOFs can be easily improved via functionalization with amino-, nitro-, hydroxy-, cyano-, or thiol-related functionalities.[54] However, the efficacy as well as the simplicity depend even more strongly on the pore topology.[55-56]

4. Conclusions and outlook

The foregoing results demonstrate that DES based on urea derivatives can be successfully employed for the ionothermal synthesis of Mg-MOF-74 with a striking impact on the crystal morphology and sorption properties. Interestingly, while the synthesis of this MOF is rather straightforward in the ChCl:urea (1:2) reline DES, higher temperatures and longer reaction duration were necessary in the e-urea based analogous solvent. Indeed, in the latter, a variety of intermediate crystalline phases could be observed and characterized by single-crystal X-ray diffraction. In these compounds, coordination of the DES components – the chloride anion and e-urea derivative – was found to compete with binding to the carboxylate. In this respect, a partial and selective deprotonation to the dobdcH_2 form was observed, leaving the hydroxyl groups uncoordinated. It was rationalized that this difference in the synthetic conditions and in the isolation of intermediate systems originates from the varying decomposition kinetics of the DES and hence from the basicity of the solvent. In reline, faster decomposition and release of ammonia favours complete deprotonation of the dobdcH_4 and the subsequent formation of the desired Mg-

MOF-74. In contrast, such decomposition process is much slower in the e-urea system leading to a stepwise deprotonation (of the carboxylic acid and phenolic protons of the dobdcH_4 linker) and the resulting observation of intermediate compounds. Although crystallographically and chemically the same material is obtained as ascertained by powder X-ray diffraction, TGA, DSC, infra-red spectroscopy and elemental analysis, the final crystalline morphology is dependent on the nature of the solvent. Whereas the classical rod-like shape is observed in reline, an unusual morphology reminiscent of a shish-kebab organization is present in the e-urea based DES. It was once again demonstrated that varying basicity of the medium was at stake in this phenomenon with a possible maturation towards Mg-MOF-74 from one of the observed intermediate phases involving the partially deprotonated ligand. This leads to a MOF with a higher specific surface area and CO_2 uptake for the material featuring this unusual morphology associated with a higher microporosity.

These results demonstrate not only the capacity of DES to allow the preparation of this MOF but also their influence on the resulting morphology and sorption properties. This opens an avenue of research by investigation of the synthesis and characterization of other known and prototypical MOFs as well as of novel materials. For example, preliminary work indicates that the analogous Ni-MOF-74 could be prepared in the DESs studied herein, whereas the Zn-MOF-74 could not be isolated under these conditions. These studies are currently on-going in our group and will be published in due course.

CRediT authorship contribution statement

Investigation: M. T., R. A. M., S. S., S. A. B.; methodology: M. T., R. A. M. and S. A. B.; writing – original draft: R.A.M., S. A.B.; writing – review & editing: M. T., S. S., R. A. M. and B. L.; funding acquisition: B. L. and S. A. B.

Declaration of competing interest

The authors declare that they have no known competing financial interests or personal relationships that could have appeared to influence the work reported in this paper.

Acknowledgments

This work has benefited from support provided by the University of Strasbourg Institute of Advanced Study (USIAS), within the French national programme “Investment for the future” (IdEx-Unistra). We also thank the Université de Strasbourg, the C.N.R.S., and the Ministère de l’Enseignement Supérieur, de la Recherche et de l’Innovation for financial support. We thank Prof. Sylvie Ferlay (Université de Strasbourg) for assistance in the DSC analysis.

Appendix A. Supplementary data

Supplementary data (XRPD, IR, DSC, BET) to this article can be found online.

References

[1] H. C. Zhou, J. R. Long, O. M. Yaghi, Introduction to metal–organic frameworks, Chem. Rev. 112 (2012) 673-674. https://doi.org/10.1021/cr300014x

[2] H. C. J. Zhou, S. Kitagawa, Metal–organic frameworks (MOFs), Chem. Soc. Rev. 43 (2014) 5415-5418. https://doi.org/10.1039/c4cs90059f

[3] M. Dincă, J. R. Long, Introduction: porous framework chemistry, Chem. Rev. 120 (2020) 8037-8038. https://doi.org/10.1021/acs.chemrev.0c00836

[4] T. Stolar, K. Užarević, Mechanochemistry: an efficient and versatile toolbox for synthesis, transformation, and functionalization of porous metal–organic frameworks, CrystEngComm 22 (2020) 4511-4525. https://doi.org/10.1039/d0ce00091d

[5] N. A. Khan, S. H. Jhung, Synthesis of metal-organic frameworks (MOFs) with microwave or ultrasound: rapid reaction, phase-selectivity, and size reduction, Coord. Chem. Rev. 285 (2015) 11-23. https://doi.org/10.1016/j.ccr.2014.10.008

[6] N. Stock, S. Biswas, Synthesis of metal-organic frameworks (MOFs): routes to various MOF topologies, morphologies, and composites, Chem. Rev. 112 (2012) 933-969. https://doi.org/10.1021/cr200304e

[7] J. Ren, X. Dyosiban N. Musyoka, H. W. Langmi, M. Mathe, S. Liao, Review on the current practices and efforts towards pilot-scale production of metal-organic frameworks (MOFs), Coord. Chem. Rev. 352 (2017) 187-219. https://doi.org/10.1016/j.ccr.2017.09.005

[8] H. Reinsch, “Green” synthesis of metal-organic frameworks, Eur. J. Inorg. Chem. (2016) 4290-4299. https://doi.org/10.1002/ejic.201600286

[9] J. Chen, K. Shen, Y. Li, Greening the processes of metal–organic framework synthesis and their use in sustainable catalysis, ChemSusChem 10 (2017) 3165-3187. https://doi.org/10.1002/cssc.201700748

[10] S. Wang, C. Serre, Toward green production of water-stable metal–organic frameworks based on Hhigh-valence metals with low toxicities, ACS Sustainable Chem. Eng. 7 (2019) 11911-11927. https://doi.org/10.1021/acssuschemeng.9b01022

[11] E. R. Engel, J. L. Scott, Advances in the green chemistry of coordination polymer materials. Green Chem. 22 (2020) 3693-3715. https://doi.org/10.1039/d0gc01074j

[12] E. Parnham, R. E. Morris, Ionothermal synthesis of zeolites, metal–organic frameworks, and inorganic–organic hybrids, Acc. Chem. Res. 40 (2007) 1005-1013. https://doi.org/10.1021/ar700025k

[13] R. E. Morris, Ionothermal synthesis — ionic liquids as functional solvents in the preparation of crystalline materials, Chem. Commun. (2009) 2990-2998. https://doi.org/10.1039/b902611h

[14] B. Zhang, J. Zhang, B. Han, Assembling metal–organic frameworks in ionic liquids and supercritical CO_2, Chem. Asian J. 11 (2016) 2610-2619. https://doi.org/10.1002/asia.201600323

[15] P. Li, F.-F. Cheng, W.-W. Xiong, Q. Zhang, New synthetic strategies to prepare metal–organic frameworks, Inorg. Chem. Front. 5 (2018) 2693-2708. https://doi.org/10.1039/c8qi00543e

[16] R. A. Maia, B. Louis, S. A. Baudron, Deep eutectic solvents for the preparation and post-synthetic modification of metal- and covalent organic frameworks, CrystEngComm 23 (2021) 5016-5032. https://doi.org/10.1039/d1ce00714a

[17] Q. Zhang, K. De Oliveira Vigier, S. Royer, F. Jérôme, Deep eutectic solvents: syntheses, properties and applications, Chem. Soc. Rev. 41 (2012) 7108-7146. https://doi.org/10.1039/c2cs35178a

[18] C. Ruß, B. König, Low melting mixtures in organic synthesis – an alternative to ionic liquids? Green Chem. 14 (2012) 2969-2982. https://doi.org/10.1039/c2gc36005e

[19] M. Francisco, A. van den Bruinhorst, M. C. Kroon, Low-transition-temperature mixtures (LTTMs): a new generation of designer solvents, Angew. Chem. Int. Ed. 52 (2013) 3074–3085. https://doi.org/10.1002/anie.201207548

[20] E. L. Smith, A. P. Abbott, K. S. Ryder, Deep eutectic solvents (DESs) and their applications, Chem. Rev. 114 (2014) 11060–11082. https://doi.org/10.1021/cr300162p

[21] B. Gurkan, H. Squire, E. Pentzer, Metal-free deep eutectic solvents: preparation, physical properties, and significance, J. Phys. Chem. Lett. 10 (2019) 7956–7964. https://doi.org/10.1021/acs.jpclett.9b01980

[22] M. A. R. Martins, S. P. Pinho, J. A. P. Coutinho, Insights into the nature of eutectic and deep eutectic mixtures, J. Sol. Chem. 48 (2019) 962-982. https://doi.org/10.1007/s10953-018-0793-1

[23] B. B. Hansen, St. Spittle, B. Chen, D. Poe, Y. Zhang, J. M. Klein, A. Horton, L. Adhikari, T. Zelovich, B. W. Doherty, B. Gurkan, E. J. Maginn, A. Ragauskas, M. Dadmun, T. A. Zawodzinski, G. A. Baker, M. E. Tuckerman, R. F. Savinell, J. R. Sangoro, Deep eutectic solvents: a review of fundamentals and applications, Chem. Rev. 121 (2021) 1232-1285. https://doi.org/10.1021/acs.chemrev.0c00385

[24] D. Yu, Z. Xue, T. Mu, Eutectics: formation, properties, and applications, Chem. Soc. Rev. 50 (2021) 8596-8638. https://doi.org/10.1039/d1cs00404b

[25] A. P. Abbott, G. Capper, D. L. Davies, R. K. Rasheed, V. Tambyrajah, Novel solvent properties of choline chloride/urea mixtures, Chem. Commun. (2003) 70-71. https://doi.org/10.1039/b210714g

[26] E. R. Parnham, E. A. Drylie, P. S. Wheatley, A. M. Z. Slawin, R. E. Morris, Ionothermal materials synthesis using unstable deep-eutectic solvents as template-delivery agents, Angew. Chem. Int. Ed. 45 (2006) 4962-4966. https://doi.org/10.1002/anie.200600290

[27] J. Zhang, T. Wu, S. Chen, P. Feng, X. Bu, Versatile structure-directing roles of deep-eutectic solvents and their implication in the generation of porosity and open metal Sites for gas storage, Angew. Chem. Int. Ed. 48 (2009) 3486-3490. https://doi.org/10.1002/anie.200900134

[28] R. A. Maia, B. Louis, S. A. Baudron, HKUST-1 MOF in reline deep eutectic solvent: synthesis and phase transformation, Dalton Trans. 50 (2021) 4145-4151. https://doi.org/10.1039/d1dt00377a

[29] S. S. Y. Chui, S. M. F. Lo, J. P. H. Charmant, A. G. Orpen, I. D. Williams, Chemically functionalizable nanoporous material $[Cu_3(TMA)_2(H_2O)_3]_n$, Science 283(1999) 1148–1150. https://doi.org/10.1126/science.283.5405.1148

[30] N. L. Rosi, J. Kim, M. Eddaoudi, B. Chen, M. O'Keeffe, O. M. Yaghi, Rod packings and metal−organic frameworks constructed from rod-shaped secondary building units, J. Am. Chem. Soc. 127 (2005) 1504-1518. https://doi.org/10.1021/ja045123o

[31] P. D. C. Dietzel, R. E. Johnsen, R. Blom, H. Fjellvåg, Structural changes and coordinatively unsaturated metal atoms on dehydration of honeycomb analogous microporous metal–organic frameworks, Chem. Eur. J. 14 (2008) 2389-2397. https://doi.org/10.1002/chem.200701370

[32] S. R. Caskey, A. G. Wong-Foy, A. J. Matzger, Dramatic tuning of carbon dioxide uptake via metal substitution in a coordination polymer with cylindrical pores, J. Am. Chem. Soc. 130 (2008) 10870-10871. https://doi.org/10.1021/ja8036096

[33] H. Wu, W. Zhou, T. Yildirim, High-capacity methane storage in metal−organic frameworks M_2(dhtp): the important role of open metal sites, J. Am. Chem. Soc. 131 (2009) 4995-5000. https://doi.org/10.1021/ja900258t

[34] H. Kim, C. S. Hong, MOF-74-type frameworks: tunable pore environment and functionality through metal and ligand modification, CrystEngComm 23 (2021) 1377-1387. https://doi.org/10.1039/d0ce01870h

[35] T. Xiao, D. Liu, The most advanced synthesis and a wide range of applications of MOF-74 and its derivatives, Micropor. Mesopor. Mater. 283 (2019) 88-103. https://doi.org/10.1016/j.micromeso.2019.03.002

[36] L. Garzón-Tovar, A. Carné-Sánchez, C. Carbonell, I. Imaz, D. Maspoch, Optimised room temperature, water-based synthesis of CPO-27-M metal–organic frameworks with high space-time yields, J. Mater. Chem. A 3 (2015) 20819-20826. https://doi.org/10.1039/c5ta04923g

[37] Z.-F. Wu, B. Hu, M.-L. Feng, X.-Y. Huang, Y.-B Zhao, Ionothermal synthesis and crystal structure of a magnesium metal-organic framework, Inorg. Chem. Commun. 14 (2011) 1132-1135. https://doi.org/10.1016/j.inoche.2011.04.006

[38] Z.-F. Wu, M.-L. Feng, B. Hu, B. Tan, X.-Y. Huang, Ionothermal synthesis of a metal-organic framework constructed by magnesium(II) and 4,4′-oxybis(benzoic acid) ligand, Inorg. Chem. Commun. 24 (2012) 166-169. https://doi.org/10.1016/j.inoche.2012.06.024

[39] G. M. Sheldrick, Crystal structure refinement with SHELXL, Acta Cryst. C 71 (2015) 3-8. https://doi.org/10.1107/s2053229614024218

[40] G. Ayoub, B. Karadeniz, A. J. Howarth, O. K. Farha, I. Đilović, L. S. Germann, R. E. Dinnebier, K. Užarević, T. Friščić, Rational synthesis of mixed-metal microporous metal–organic frameworks with controlled composition using mechanochemistry, Chem. Mater. 31 (2019) 5494-5501. https://doi.org/10.1021/acs.chemmater.9b01068

[41] D. R. Du Bois, K. R. Wright, M. K. Bellas, N. Wiesner, A. J. Matzger, Linker deprotonation and structural evolution on the pathway to MOF-74, Inorg. Chem. 61 (2022) 4550–4554. https: doi.org/10.1021/acs.inorgchem.1c03988

[42] M. Teixeira, R. A. Maia, L. Karmazin, B. Louis, S. A. Baudron, Ionothermal synthesis of calcium-based metal–organic frameworks in a deep eutectic solvent, CrystEngComm 24 (2022) 601-608. https://doi.org/10.1039/d1ce01497h

[43] S. E. Henkelis, S. M. Vornholt, D. B. Cordes, A. M. Z. Slawin, P. S. Wheatley, R. E. Morris, A single crystal study of CPO-27 and UTSA-74 for nitric oxide storage and release, CrystEngComm 21 (2019) 1857-1861. https://doi.org/10.1039/c9ce00098d

[44] A. Keller, Unusual orientation phenomena in polyethylene interpreted in terms of the morphology, J. Polym. Sci. 15 (1955) 31-49. https://doi.org/10.1002/pol.1955.120157904

[45] S. P. Simeonov, C. A. M. Afonso, Basicity and stability of urea deep eutectic mixtures, RSC Adv. 6 (2016) 5485-8490. https://doi.org/10.1039/c5ra24558c

[46] L. Feng, J.-L. Li, G. S. Day, X.-L. Lv, H.-C. Zhou, Temperature-controlled evolution of nanoporous MOF crystallites into hierarchically porous superstructures. Chem 5 (2019) 1265-1274. https://doi.org/10.1016/j.chempr.2019.03.003

[47] E. A. Drylie, D. S. Wragg, E. R. Parnham, P. S. Wheatley, A. M. Z. Slawin, J. E. Warren, R. E. Morris, Ionothermal synthesis of unusual choline-templated cobalt aluminophosphates, Angew. Chem., Int. Ed. 46 (2007) 7839–7843. https://doi.org/10.1002/ange.200702239

[48] K. Sumida, D. L. Rogow, J. A. Mason, T. M. McDonald, E. D. Bloch, Z. R. Herm, T.-H Bae, J. R. Long, Carbon dioxide capture in metal–organic frameworks, Chem. Rev. 112 (2012) 724-781. https://doi.org/10.1021/cr2003272.

[49] C. A. Trickett, A. Helal, B. A. Al-Maythalony, Z. H. Yamani, K. E. Cordova, O. M. Yaghi, The chemistry of metal–organic frameworks for CO_2 capture, regeneration and conversion. Nature Reviews Materials 2 (2017) 1-16. https://doi.org/10.1038/natrevmats.2017.45

[50] M.-M. Jin, Y.-X. Li, C. Gu, X.-Q. Liu, L.-B. Sun, Tailoring microenvironment of adsorbents to achieve excellent CO_2 uptakes from wet gases, AIChe J. 66 (2020) e16645. https://doi.org/10.1002/aic.16645

[51] D.-A. Yang, H.-Y, Cho, J. Kim, S.-T. Yang, W. S. Ahn, CO_2 capture and conversion using Mg-MOF-74 prepared by a sonochemical method, Energy Environ. Sci. 5 (2012) 6465-6473. https://doi.org/10.1039/c1ee02234b

[52] Z. Bao, L. Yu, Q. Ren, X. Lu, S. Deng, Adsorption of CO_2 and CH_4 on a magnesium-based metal organic framework, J. Colloid Interface Sci. 353 (2011) 549-556. https://doi.org/10.1016/j.jcis.2010.09.065

[53] C. Wu, L.-Y. Chou, L. Long, X. Si, W.-S. Lo, C.-K. Tsung, T. Li, Structural control of uniform MOF-74 microcrystals for the study of adsorption kinetics, ACS Appl. Mater. Interfaces 11 (2019) 35820–35826. https://doi.org/10.1021/acsami.9b13965

[54] W. Gao, S. Liang, R. Wang, Q. Jiang, Y. Zhang, Q. Zheng, B. Xie, C. Ying Toe, X. Zhu, J. Wang, L. Huang Y. Gao, Z. Wang, C. Jo, Q. Wang, L. Wang, Y. Liu, B. Louis, J. Scott, A.-C. Roger, R. Amal, H. Heh, S.-E. Park, Industrial carbon dioxide capture and utilization: state of the art and future challenges, Chem. Soc. Rev. 49 (2020) 8584–8686. https://doi.org/10.1039/d0cs00025f

[55] R. Anderson, J. Rodgers, E. Argueta, A. Biong, D. A. Gomez-Gualdron, Role of pore chemistry and topology in the CO_2 capture capabilities of MOFs: from molecular simulation to machine learning, Chem. Mater. 30 (2018) 6325–6337. https://doi.org/10.1021/acs.chemmater.8b02257

[56] C. E. Bien, K. K. Chen, S.-C. Chien, B. R. Reiner, L.-C. Lin, C. R. Wade, W. S. W. Ho, Bioinspired metal–organic framework for trace CO_2 capture. J. Am. Chem. Soc. 140 (2018) 12662–12666. https://doi.org/10.1021/jacs.8b06109